18. Friedrich, B. *et al.* Towards magnetic trapping of molecules. *J. Chem. Soc. Faraday Trans.* **94,** 1783–1791 (1998).
19. Wing, W. H. Electrostatic trapping of neutral atomic particles. *Phys. Rev. Lett.* **45,** 631–634 (1980).
20. Gandhi, S. R. & Bernstein, R. B. Focusing and state selection of NH_3 and OCS by the electrostatic hexapole via first- and second-order Stark effects. *J. Chem. Phys.* **87,** 6457–6467 (1987).
21. Ashfold, M. N. R., Dixon, R. N., Little, N., Stickland, R. J. & Western, C. M. The B^1E'' state of ammonia: sub-Doppler spectroscopy at vacuum ultraviolet energies. *J. Chem. Phys.* **89,** 1754–1761 (1988).
22. Bahns, J. T., Gould, P. L. & Stwalley, W. C. Formation of cold ($T \leq 1$ K) molecules. *Adv. At. Mol. Opt. Phys.* **42,** 171–224 (2000).

Acknowledgements

This work is part of the research program of the 'Stichting voor Fundamenteel Onderzoek der Materie (FOM)', which is financially supported by the 'Nederlandse Organisatie voor Wetenschappelijk Onderzoek (NWO)'. The research of R.T.J. has been made possible by a fellowship of the Royal Netherlands Academy of Arts and Sciences. We acknowledge the technical assistance of Ch. Timmer.

Correspondence and requests for information should be addressed to G.M. (e-mail: gerardm@rijnh.nl).

Quasi-planar nucleus structure in apoferritin crystallization

S.-T. Yau* & Peter G. Vekilov*†

* *Center for Microgravity and Materials Research, and* †*Department of Chemistry, University of Alabama in Huntsville, Huntsville, Alabama 35899, USA*

First-order phase transitions of matter, such as condensation and crystallization, proceed through the formation and subsequent growth of 'critical nuclei' of the new phase. The thermodynamics and kinetics of the formation of these critical nuclei depend on their structure, which is often assumed to be a compact, three-dimensional arrangement of the constituent molecules or atoms[5,6]. Recent molecular dynamics simulations have predicted compact nucleus structures for matter made up of building blocks with a spherical interaction field[7,8], whereas strongly anisotropic, dipolar molecules may form nuclei consisting of single chains of molecules[9]. Here we show, using direct atomic force microscopy observations, that the near-critical-size clusters formed during the crystallization of apoferritin, a quasi-spherical protein, and which are representative of the critical nucleus of this system, consist of planar arrays of one or two monomolecular layers that contain 5–10 rods of up to 7 molecules each. We find that these clusters contain between 20 and 50 molecules each, and that the arrangement of the constituent molecules is identical to that found in apoferritin crystals. We anticipate that similarly unexpected critical nucleus structures may be quite common, particularly with anisotropic molecules, suggesting that advanced nucleation theories should treat the critical nucleus structure as a variable.

Protein crystallization is a convenient model for studies of molecular structures and dynamics of nucleation: protein molecules' sizes (a few nanometres) and the typical timescales for growth (a few seconds between sequential discrete growth events) are within the reach of current surface characterization techniques. The molecules of our model, apoferritin[10], are quasi-spherical and consist of 24 subunits arranged in pairs along the 12 walls of a quasi-rhombododecahedron[11,12]. Apoferritin crystals have a face-centred cubic (f.c.c.) lattice, faceted by hexagonal [111] planes[13,14].

We monitored large crystals for periods of several hours in the range of supersaturations σ from 0.5 to 1.6 (for experimental procedures and definition of σ, see Methods below), and detected clusters landing on the top (111) crystal surfaces. Figures 1a and 2a, taken a few minutes after cluster landing, show examples representative of more than 15 such events. In all cases, the molecules in a cluster are arranged in rows of 4–8 molecules, while 3–7 rows assemble in planar domains with an additional 2–3 rows forming a second layer. The cluster in Fig. 1 contains two domains linked by a longer row of about 10 molecules. The centre-to-centre distance between adjacent molecules in a row is 13 nm, equal to that along the close-packed ⟨110⟩ direction in the crystal. Furthermore, one of the molecular rows of the cluster in Fig. 2 generates a new (111) layer that spreads on the crystal surface to meet the crystal's own layer. Hence, these are clusters of apoferritin molecules, which, unlike occurrences in other systems[15,16], have the same arrangement as in the crystal.

The quasi-planar cluster shape precludes the clusters being pieces chopped off a large crystal. We conclude that the clusters form in the solution bulk and then land on the monitored surface because: (1) the clusters consist of (110) planes (Fig. 1f) rather than (111) planes, typical of 'two-dimensional' nuclei of new layers replicating the (111) molecular arrangement of the crystal surface[14]. (2) The molecular rows in the cluster in Fig. 1 are at an angle to the crystal's ⟨110⟩ direction. (3) The cluster and the layer originating from it in Fig. 2 are out of registry with the crystal's own layer causing a boundary free of molecules or consisting of strained molecules. (4) Often—see for instance Fig. 1e—the clusters are pushed back into the solution by the advancing crystal layers. (5) If trapped by the crystal layers[17], as in Fig. 2e and f, a misfit boundary between the two structures appears. Did the cluster structure change after landing, under the influence of the translationally symmetric force exerted by the underlying crystal? It seems not: we would expect that in such a case there would be an exact match and continuity between the structures of the cluster and the underlying crystal, as observed before[15,18].

Figures 1 and 2 show that molecules attach to, and detach from, the cluster between two frames. The attachment and detachment frequencies are comparable, which is unusual for the supersaturated conditions of the observation (we note the fast advancing long straight steps in Fig. 1d and e, and Fig. 2e and f). Comparable rates of molecular attachment and detachment, and bifurcation of their subsequent evolution into either growth or dissolution were observed for all clusters of such sizes seen in our experiments. Estimating the average net frequency of molecular attachment in Fig. 1, we get about 4 molecules/43 s $\approx 0.1\ s^{-1}$ for the approximately 20 possible attachment sites at the ends of the molecular rows, or $0.005\ s^{-1}$ per attachment site. This frequency is more than an order of magnitude lower than the net frequency of attachment to a growth site on the surface of a large crystal—$0.065\ s^{-1}$ (ref. 14). The ratio of the two rates indicates that the size of the cluster in Fig. 1 is just above the critical size. The cluster in Fig. 2 loses one layer of 6 molecules in 896 s (compare Fig. 2a and d). Hence, its size must be just below the critical for that supersaturation. We conclude that these are near-critical-size clusters for the phase transformation occurring in the system, crystallization of apoferritin. Their sizes are, respectively, larger and smaller than the critical, and their structure should be representative of the structure of the nucleus.

The size of the near-critical cluster in Fig. 2 at $\sigma = 1.6$ decreases from about 25 to about 20 molecules during the monitoring time. This cluster is smaller than the one in Fig. 1 at $\sigma = 1.1$ which contains about 50–60 molecules. On the average, smaller near-critical clusters were observed at higher supersaturations. Although we do not have sufficient statistics for a quantitative statement, these observations agree with the predictions of the classical and advanced treatments of nucleation[1,2,19].

To eliminate possible effects of the large crystals on the nucleation pathways, we viewed the glass bottom of the atomic force microscope (AFM) cell before the formation of any crystals at σ between 0.5 and about 2.5. A disordered apoferritin layer with roughly hexagonal molecular co-ordination covers the glass. We saw numer-

© 2000 Macmillan Magazines Ltd

ous clusters ranging from 2–3 to 50–70 molecules (we never saw single molecules) that land on the apoferritin-covered glass, stay adsorbed for 1 to 30 min and then dissolve or desorb. Typically, smaller clusters had significantly shorter residence times on the surface. Hence, although the occurrence of smaller clusters appeared higher, comparisons of the populations of large and small clusters with theoretical predictions would be unjustified. We noted that: (1) in the smallest clusters the molecules occupy the corners of a polygon. (2) Clusters of about 10–20 molecules consist of two parallel molecular rows. (3) Two structures were possible for clusters of 20 or more molecules: a few molecular rows in a plane, or disordered aggregates. (4) Apoferritin molecules detached from the

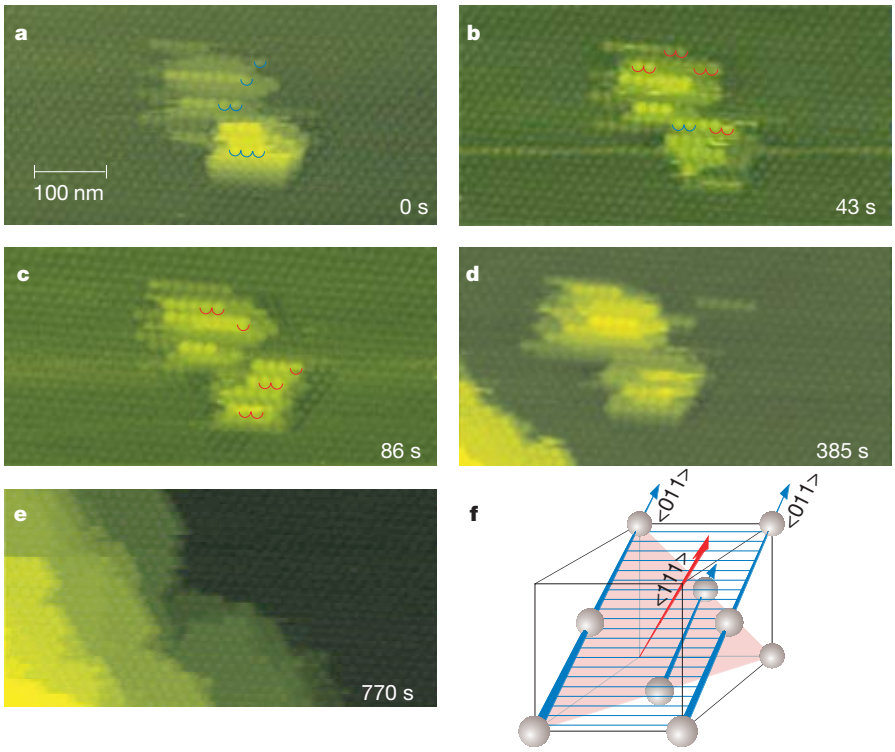

Figure 1 Near-critical-size cluster on the (111) face of an apoferritin crystal at supersaturation $\sigma = 1.1$. **a**–**c**, Molecules attach and detach from the cluster. Molecules that are missing in the next frame are highlighted in blue, those that have appeared after the previous frame was captured are highlighted in red. **d**, **e**, An advancing step pushes the cluster back into the solution. The step velocity is 0.6 nm s^{-1}, close to the fastest step velocity previously recorded for this supersaturation with apoferritin crystals[14]. This indicates that the selected AFM imaging mode did not affect the monitored processes. **f**, Diagram of (111) and (110) planes and ⟨110⟩ molecular rows in a face-centred cubic (f.c.c.) crystal lattice.

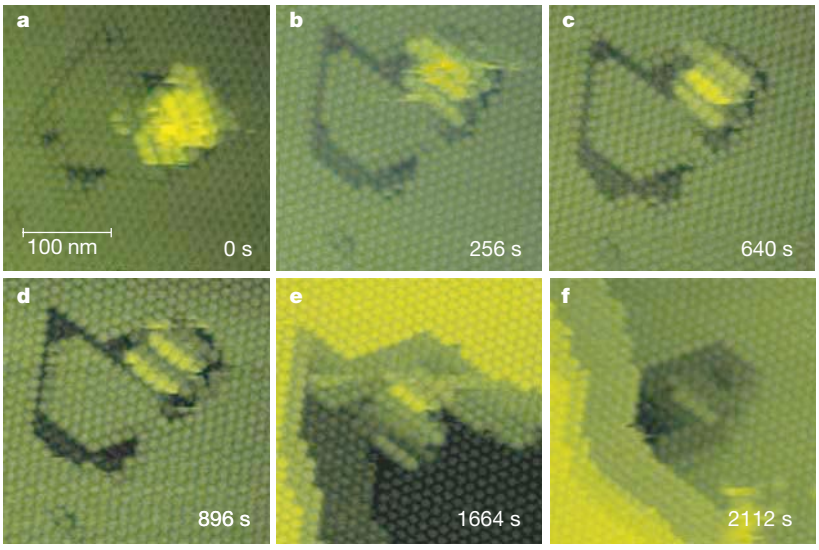

Figure 2 A slowly dissolving cluster at $\sigma = 1.6$. **a**–**d**, The top layer of the cluster is gradually disappearing because more molecules detach than attach to the cluster. The fraction of the top crystal layer originating from the cluster is out of registry with the remaining part. **e**, **f**, A few steps belonging to the crystal surround the cluster. Note the misfit between the molecules of the crystal and the molecules of the cluster. The direction of scanning was changed between **a** and **b**. The consistency of the cluster structure is evidence for the lack of AFM imaging artefacts.

© 2000 Macmillan Magazines Ltd

ordered clusters, while (5) the disordered ones were inactive. (6) The larger ordered clusters were not seen at the high supersaturations. We conclude that the clusters in (1)–(4) above are the subcritical clusters that constitute the stages in the nucleation process preceding those seen in Figs 1 and 2.

Figure 3 shows that the clusters that form in the solution may develop into (111) faceted f.c.c. crystals. We see a microcrystal that consists of three (111) layers of about 60 molecules in each. The inclination of the microcrystals indicates that it was formed in the solution bulk and later landed in our field of view. Clusters similar to those in Figs 1 and 2 can evolve to such a microcrystal by accumulating several (110) layers until a (111) face is formed.

The nucleation pathway emerging from the above observations is schematically summarized in Fig. 4. The (110) planar—rather than compact as in Fig. 4b—structure of the nucleus is surprising[5,6]. At present, in analogy to the case of anisotropic dipolar molecules[9], we can only speculate that the slight anisotropy of the apoferritin molecules, either directly, or after enhancement by the formation of a two-member cluster, underlies the observed shape.

This nucleus structure may have important consequences for the nucleation process. A planar cluster has a larger surface area than a compact cluster with the same number of molecules n. As a result, a larger contribution to the crystallization energy gain is needed to compensate for the greater surface energy loss, and hence the number of molecules in the critical cluster n^* is greater. Because the nucleation barrier $\Delta G^*(n^*) \approx n^*\Delta\mu/2$ (refs 5, 19–21), the higher nucleation barriers lead to slower nucleation kinetics than predicted by the classical theories based on compact spherical nuclei. Furthermore, the rough surface of the nuclei in Figs 1–3 may result in a surface energy that is not a smooth and monotonic function of n. This may result in unusual dependencies of the nucleation rate on $\Delta\mu$.

To quantitatively characterize the nucleation process, we use the fact (see Figs 3 and 4a), that the nucleus evolves into a crystal by accumulating new layers. Following refs 22 and 23, we find that the contribution to the partial molecular surface free energy associated with the equilibrium addition of a (110) layer consisting of $n_e \times n_e$ molecules to a (110) cluster surface is $2\phi/n_e$. Here ϕ is the free energy of the intermolecular bond in the crystals (the entropic components stem from the water molecules trapped in the crystal or bound to the solute; S.-T.Y. *et al.*, manuscript in preparation). For a critical cluster in labile equilibrium with the solution, this excess free energy is balanced by the supersaturation, that is, $\Delta\mu = 2\phi/n_e$ (the Gibbs–Thomson equation[22,23]). Substituting $\phi/k_BT = 3.2$ (ref. 14), with $\Delta\mu/k_BT = 1.1$ and 1.6, the values of n_e are 6 and 4, respectively, that is, approximately the cluster sizes in Figs 1 and 2. Hence, ϕ is the molecular-level equivalent to surface tension that governs nucleation[22].

Comparing the n_e values with the respective n^* values indicated above, we find that $n^* \approx n_e^{2.3}$. Extrapolating to $\Delta\mu/k_BT = 3.8$, at which apoferritin crystals are typically grown[13], we get $n_e \approx 1$ or 2, $n^* \approx 3$–4 (for structures of such clusters imaged by atomic force microscopy at lower σ values, see above). Assuming a pre-exponential factor for the nucleation rate law $J_0 \approx 1\,\mathrm{cm^{-3}\,s^{-1}}$ (for lysozyme, J_0 is between 1 and $10\,\mathrm{cm^{-3}\,s^{-1}}$; refs 24, 25) and using, as above, $\Delta G^* = n^*\Delta\mu/2$, we get for the nucleation rate $J = J_0\exp[-\Delta G^*(n^*)/k_BT] \approx 10^{-3}\,\mathrm{cm^{-3}\,s^{-1}}$. In an overnight experiment with a few hundred microlitres of solution, about 10 crystals should nucleate. Accordingly, numerous experiments under these conditions produced between a few and about 100 crystals.

To compare the estimated ϕ to previous results, we define a corresponding effective macroscopic surface energy γ as $n_{free}\phi/S$. Here n_{free} is the number of unsaturated bonds of a molecule on the surface of a nucleus, and S is the surface area of a molecule. With n_{free} being on average 7–8 for the clusters that expose two sides of many molecules, (see Figs 1 and 2) we get $\gamma \approx 0.2\,\mathrm{mJ\,m^{-2}}$. Light-scattering determinations of apoferritin nuclei sizes averaged over all body angles[26] at $\sigma = 0.92$ yielded values of about 40 nm (or ~3.5 molecular dimensions, compatible with the cluster in Fig. 1). Assuming a spherical nucleus shape, a value of $\gamma = 0.027\,\mathrm{mJ\,m^{-2}}$ was obtained[26]. As discussed above, for a spherical cluster n_{free} is lower than for a flat cluster with the same n_e. Hence, the surface energy value resulting from this assumption is also lower. Similarly, AFM studies of virus crystallization kinetics[27] produced γ-values

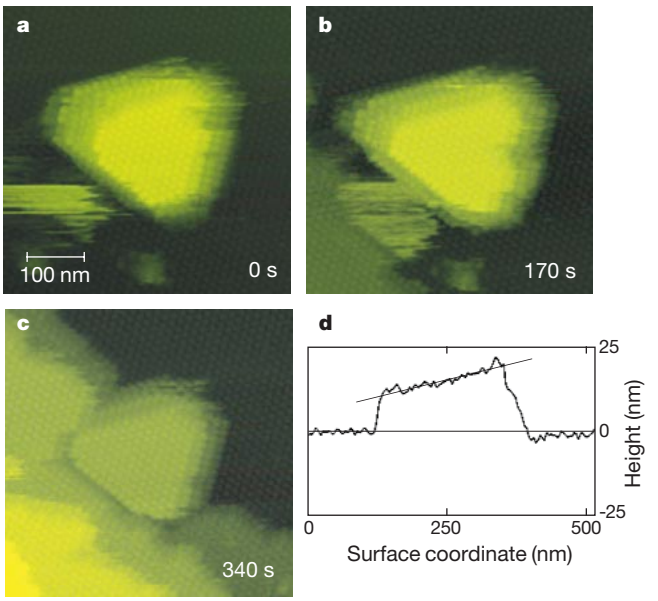

Figure 3 Microcrystal at $\sigma = 1.1$. **a**–**c**, The microcrystal slowly grows by attachment of molecules to the side (110) faces, while a step belonging to the crystal moves rapidly to incorporate it. **d**, Height profile along a line roughly from top left to bottom right in **a** shows that the microcrystal is inclined with respect to the substrate by about 3°. This corresponds to one molecule trapped under the microcrystal close to its edge or to an unfinished layer on its bottom surface.

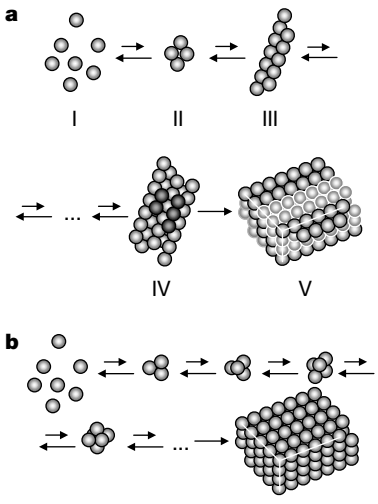

Figure 4 Schematic illustration of nucleation pathways. **a**, Nucleation via a planar critical cluster. Stage I, single molecules in the solution; the lack of any significant concentration of dimers, trimers, and so on, has been shown by static and dynamic light scattering[28,29]. Stage II, a few molecules at the corners of a polygon. Stage III, linear array. Stage IV, a quasi-planar critical cluster with (110) orientation, similar to structures seen in Figs 1 and 2; molecules belonging to the second layer are shown in a lighter shade. Stage V, microcrystal faceted by (111) planes; the (110) layers that stack up to form this crystal are delineated by lighter and darker contours. **b**, Nucleation via a compact critical cluster[5,6].

© 2000 Macmillan Magazines Ltd

higher by about the same factor than the evaluation based on light scattering[26]. □

Methods

Monitoring was performed *in situ* in the AFM fluid cell at 23.0 ± 0.3 °C maintained by stabilizing the room temperature. This temperature was higher by 0.5–1 °C than the setting in the room. The insensitivity of apoferritin crystallization to temperature variations[13] justifies this approach to temperature control. We used the less intrusive tapping mode of the AFM and a tip with minimal force constant. The scanning parameters were adjusted such that continuous imaging affected neither the surface structure, nor the process dynamics. For verification, we varied the scan sizes and the time elapsed between image collections, and saw that neither the spatial nor the temporal characteristics of the monitored processes changed. Supersaturation σ, defined as chemical potential difference $\Delta\mu$ (in k_BT units) between the solution and a large crystal, was calculated from the actual and equilibrium solution concentrations, C and C_e: $\sigma \equiv \Delta\mu/k_BT = \ln(C/C_e)$. The effects on solution non-ideality on this determination of $\Delta\mu$ are minor for this system (S.-T.Y. *et al.*, manuscript in preparation). This $C_e = 23 \pm 3\ \mu g\ cm^{-3}$ was determined as the value of C at which long steps stopped moving, before retreating in solutions of $C < C_e$. The (111) surface provides a scale for determinations of the dimensions of the clusters. The periodicity within a molecular row along a ⟨110⟩ direction is 13 nm, and the layer thickness is 10.5 nm, in good agreement with the X-ray structure[11,12].

AFM, a surface characterization technique, can be applied to visualize clusters that appear in the solution bulk only because they reach a surface and adsorb on it. The average brownian diffusion time τ to reach the substrate for a cluster formed within a $x = 100\ \mu m$ thick layer can be evaluated from Einstein's relation $x^2 = 2D\tau$. A lower estimate for cluster diffusivity D can be obtained from the diffusivity of single apoferritin molecules, $3.2 \times 10^{-7}\ cm^2\ s^{-1}$ (refs 28, 29), using Stokes law and assuming that the cluster behaves like a particle with seven molecules at an edge: $D \approx 5 \times 10^{-8}\ cm^2\ s^{-1}$. Substituting, $\tau \approx 1{,}000\ s \approx 15$ min. Assuming sedimentation in the Earth's gravity field[30] would lead to landing times longer by more than an order of magnitude.

We performed numerical simulations of combined buoyancy-driven convection and solute diffusion, as in ref. 31, to evaluate the concentration nonuniformity due to the crystal growth in the cell. We found that at the average rate of growth of the underlying crystal $< 0.1\ nm\ s^{-1}$, apoferritin depletion at the interface is $< 1\%$, and the characteristic diffusion and convection velocities are, respectively, $0.3\mu m\ s^{-1}$ and $< 1\ \mu m\ s^{-1}$. The AFM tip travel for scan widths of 0.5 μm and frequencies of about $3\ s^{-1}$, and the ~20-kHz tapping oscillation, could add solution flow with similar velocities. None of those should affect cluster evolution.

Received 3 September 1999; accepted 8 June 2000.

1. Gibbs, J. W. *The Collected Works of J.W. Gibbs* (Yale Univ. Press, New Haven, 1961).
2. Oxtoby, D. W. Nucleation of first order phase transitions. *Acc. Chem. Res.* **31,** 91–97 (1998).
3. Volmer, M. *Kinetik der Phasenbildung* (Steinkopff, Dresden, 1939).
4. Hill, T. L. *Thermodynamics of Small Systems* (Benjamin, New York, 1963).
5. Milchev, A. Electrochemical phase formation on a foreign substrate - basic theoretical concepts and some experimental results. *Contemp. Phys.* **32,** 321–332 (1991).
6. Chernov, A. A. *Modern Crystallography III: Growth of Crystals* (Springer, Berlin, 1984).
7. ten Wolde, P. R. & Frenkel, D. Enhancement of protein crystal nucleation by critical density fluctuations. *Science* **277,** 1975–1978 (1997).
8. Talanquer, V. & Oxtoby, D. W. Crystal nucleation in the presence of a metastable critical point. *J. Chem. Phys.* **109,** 223–227 (1998).
9. ten Wolde, P. R., Oxtoby, D. W. & Frenkel, D. Coil-globule transition in gas-liquid nucleation of polar fluids. *Phys. Rev. Lett.* **81,** 3695–3698 (1998).
10. Harrison, P. M. & Arosio, P. The ferritins: molecular properties, iron storage function and cellular regulation. *Biochim. Biophys. Acta* **1275,** 161–203 (1996).
11. Lawson, D. M. *et al.* Solving the structure of human H ferritin by genetically engineering intermolecular crystal contacts. *Nature* **349,** 541–544 (1991).
12. Hempstead, P. D. *et al.* Comparison of the three dimensional structures of recombinant human H and horse L ferritins at high resolution. *J. Mol. Biol.* **268,** 424–448 (1997).
13. Thomas, B. R., Carter, D. & Rosenberger, F. Effects of microheterogeneity on horse spleen apoferritin crystallization. *J. Cryst. Growth* **187,** 499–510 (1997).
14. Yau, S.-T., Thomas, B. R. & Vekilov, P. G. Molecular mechanisms of crystallisation and defect formation. *Phys. Rev. Lett.* **85,** 353–356 (2000).
15. Kuznetsov, Y. G., Malkin, A. J. & McPherson, A. Atomic force microscopy studies of phase separations in macromolecular systems. *Phys. Rev. B* **58,** 6097–6103 (1998).
16. Georgalis, Y., Umbach, P., Raptis, J. & Saenger, W. Lysozyme aggregation studied by light scattering. I. Influence of concentration and nature of electrolyte. *Acta Crystallogr. D* **53,** 691–702 (1997).
17. Malkin, A. J., Kuznetsov, Y. G. & McPherson, A. Defect structure of macromolecular crystals. *J. Struct. Biol.* **117,** 124–137 (1996); Incorporation of microcrystals by growing protein and virus crystals. *Proteins Struct. Funct. Genet.* **24,** 247–252 (1996).
18. Kuznetsov, Y. G., Malkin, A. J. & McPherson, A. AFM studies of the nucleation and growth mechanisms of macromolecular crystals. *J. Cryst. Growth* **196,** 489–502 (1999).
19. Mutaftschiev, B. in *Handbook of Crystal Growth* (ed. Hurle, D. T. J.) 189–247 (Elsevier, Amsterdam, 1993).
20. Kashchiev, D. On the relation between nucleation work, nucleus size, and nucleation rate. *J. Chem. Phys.* **76,** 5098–5102 (1982).
21. Oxtoby, D. W. & Kashchiev, D. A general relation between the nucleation work and the size of the nucleus in multicomponent nucleation. *J. Chem. Phys.* **100,** 7665–7671 (1994).
22. Stranski, I. N. & Kaischew, R. Über den Mechanismus des Gleichgewichtes kleiner Kriställchen. I. *Z. Phys. Chem. B* **26,** 100–113 (1934).
23. Kaischew, R. & Stranski, I. N. Über die Thomson-Gibbs'sche Gleichung bei Kristallen. *Z. Phys. Chem. B* **35,** 427–432 (1937).
24. Vekilov, P. G., Monaco, L. A., Thomas, B. R., Stojanoff, V. & Rosenberger, F. Repartitioning of NaCl and protein impurities in lysozyme crystallization. *Acta Crystallogr. D* **52,** 785–798 (1996).
25. Galkin, O. & Vekilov, P. G. Direct determination of the nucleation rate of protein crystals. *J. Phys. Chem.* **103,** 10965–10971 (1999); Are nucleation kinetics of protein crystals similar to those of liquid droplets? *J. Am. Chem. Soc.* **122,** 156–163 (2000); Control of protein crystal nucleation around the metastable liquid-liquid phase boundary. *Proc. Natl Acad. Sci. USA* **97,** 6277–6281 (2000).
26. Malkin, A. J. & McPherson, A. Light scattering investigation of the nucleation processes and kinetics of crystallization in macromolecular systems. *Acta Crystallogr. D* **50,** 385–395 (1994).
27. Malkin, A. J., Land, T. A., Kuznetsov, Yu. G., McPherson, A. & DeYoreo, J. J. Investigation of virus crystal growth mechanism by in situ atomic force microscopy. *Phys. Rev. Lett.* **75,** 2778–2781 (1995).
28. Petsev, D. N. & Vekilov, P. G. Evidence for non-DLVO hydration interactions in solutions of the protein apoferritin. *Phys. Rev. Lett.* **84,** 1339–1342 (2000).
29. Petsev, D. N., Thomas, B. R., Yau, S.-T. & Vekilov, P. G. Interactions and aggregation of apoferritin molecules in solution: effects of added electrolytes. *Biophys. J.* **78,** 2060–2069 (2000).
30. Atkins, P. *Physical Chemistry* (Freeman, New York, 1998).
31. Lin, H., Rosenberger, F., Alexander, J. I. D. & Nadarajah, A. Convective-diffusive transport in protein crystal growth. *J. Cryst. Growth* **151,** 153–162 (1995).

Acknowledgements

We thank D. W. Oxtoby, D. N. Petsev, J. I. D. Alexander, O. Galkin, S. Weinkauf, J. M. Garcia-Ruiz and N. Booth for suggestions and encouragement; B. R. Thomas for providing pure apoferritin; H. Lin and D. N. Petsev for numerical simulations; and L. Carver for graphics work. This research was supported by the National Heart, Lung, and Blood Institute, NIH, the Life and Microgravity Sciences and Applications Division of NASA, and the State of Alabama through the Centre for Microgravity and Materials Research at the University of Alabama in Huntsville.

Correspondence and requests for materials should be addressed to P.G.V. (e-mail: peter@cmmr.uah.edu).

Marine control of biological production in the eastern equatorial Pacific Ocean

Paul Loubere

Department of Geology and Environmental Geosciences, Northern Illinois University, DeKalb, Illinois 60115, USA

The eastern equatorial Pacific Ocean is the site of approximately 20–50% of new biological production in the global oceans[1]. This region is also responsible for the greatest efflux of CO_2 from oceans to the atmosphere[2]. New production, which fixes carbon in response to external inputs of nutrients as opposed to supply from local nutrient recycling, is thought to modulate the CO_2 release[3]. But what controls new production in this region is less clear. Here we present a quantitative reconstruction of biological production in the surface ocean for this region over the past 130,000 years, which shows that the equatorial Pacific Ocean exhibits higher-frequency variations than the South Equatorial Current. Comparison of these records with palaeotemperature reconstructions indicates that atmospherically driven mechanisms—such as aeolian flux of iron or wind-driven changes in upwelling rate of nutrient-rich waters—are unlikely to have influenced longer-term rates of production in this region. Instead, biological production appears to be governed by changes in ocean circulation and the chemical composition of upwelled water.

Four core locations in the eastern equatorial Pacific (EEP) were selected for palaeoproductivity reconstruction with the main objectives of discovering the regional mode(s) of productivity variation and testing for processes controlling that variation. The deep-sea cores used were (Fig. 1): RC13-110 (0.10° N, 95.65° W; 3,231 m water depth (w.d.); average sedimentation rate (a.s.r.), 2.4 cm kyr^{-1},

© 2000 Macmillan Magazines Ltd